NeuroImage 47 (2009) 1425–1434

Contents lists available at ScienceDirect

NeuroImage

journal homepage: www.elsevier.com/locate/ynimg

fMRI at 1.5, 3 and 7 T: Characterising BOLD signal changes

Wietske van der Zwaag, Susan Francis, Kay Head, Andrew Peters, Penny Gowland, Peter Morris, Richard Bowtell *

Sir Peter Mansfield Magnetic Resonance Centre, School of Physics and Astronomy, University of Nottingham, Nottingham, NG7 2RD, UK

ARTICLE INFO

Article history:
Received 12 January 2009
Revised 28 April 2009
Accepted 5 May 2009
Available online 14 May 2009

ABSTRACT

Blood oxygenation level dependent (BOLD) signal changes occurring during execution of a simple motor task were measured at field strengths of 1.5, 3 and 7 T using multi-slice, single-shot, gradient echo EPI at a resolution of $1\times1\times3$ mm^3, to quantify the benefits offered by ultra-high magnetic field for functional MRI. Using four different echo times at each field strength allowed quantification of the relaxation rate, R_2^* and the change in relaxation rate on activation, ΔR_2^*. This work adds to previous studies of the field strength dependence of BOLD signal characteristics, through its: (i) focus on motor rather than visual cortex; (ii) use of single-shot, multi-slice, gradient echo EPI for data acquisition; (iii) co-registration of images acquired at different field strengths to allow assessment of the BOLD signal changes in the same region at each field strength. ΔR_2^* was found to increase linearly with field strength (0.51 ± 0.06 s^{-1} at 1.5 T; 0.98 ± 0.08 s^{-1} at 3 T; 2.55 ± 0.22 s^{-1} at 7 T), while the ratio of $\Delta R_2^*/R_2$, which dictates the accessible BOLD contrast was also found to increase (0.042 ± 0.002 at 1.5 T; 0.054 ± 0.002 at 3 T; 0.084 ± 0.003 at 7 T). The number of pixels classified as active, the *t*-value calculated over a common region of interest and the percentage signal change in the same region were all found to peak at TE ~ T_2^* and increase significantly with field strength. An earlier onset of the haemodynamic response at higher field provides some evidence for a reduced venous contribution to the BOLD signal at 7 T.

Introduction

Magnetic resonance imaging systems operating at magnetic fields greater than 3 T are becoming increasingly widely available. A key factor driving the development of such systems has been the expectation that they will give greatly increased sensitivity to blood oxygenation level dependent (BOLD) contrast. This is based on both the expected increase in intrinsic signal to noise ratio (SNR) with field strength and also the increase in BOLD signal changes at elevated field. This increase was first demonstrated experimentally by Turner et al. (1993) and subsequently has been most fully explored by Gati et al. (1997) and Yacoub et al. (2001). The BOLD signal arises from local field inhomogeneities caused by magnetic susceptibility differences between deoxyhaemoglobin-rich blood in capillaries and venous vessels and the surrounding tissue, which scale linearly with field strength. The resulting increase in BOLD contrast is of great benefit for functional MRI (fMRI) studies and can be exploited to improve the spatial resolution, or reduce the number of trials required to demonstrate robust activation. This can facilitate the study of the response to single trials and rare events, or the investigation of subtle cognitive effects. The benefits of the increased BOLD contrast at high field can be most fully realised when the intrinsic noise in the image data is greater in magnitude than the physiological noise (Triantafyllou et al., 2005). This is because physiological noise is generally proportional to signal strength and so when this noise contribution dominates, the signal to noise ratio is independent of signal strength (Triantafyllou et al., 2005). This behaviour means that high field offers most benefit for fMRI experiments carried out at high spatial resolution, where the scaling of signal strength with voxel volume helps to reduce the relative contribution of the physiological noise (Bodurka et al., 2007; Triantafyllou et al., 2005). At higher magnetic fields, the short T_2 of blood (Yacoub et al., 2001) means that its signal is attenuated relative to that from tissue at the echo times (TEs) used for fMRI. Hence it is expected that higher spatial specificity can be obtained in BOLD data acquired at high field as the intra-vascular signal contribution from draining veins is reduced (Duong et al., 2003a; Gati et al., 1997; Ogawa et al., 1998; Yacoub et al., 2001).

There have been several previous detailed studies of BOLD signal change as a function of field strength. The majority of these have focused on the effect of field strength on the volume of activation and measures of the strength of activation such as the percentage signal change or average *t*-score (Duong et al., 2003b; Fera et al., 2004; Gati et al., 1997; Krasnow et al., 2003; Turner et al., 1993; Yacoub et al., 2001; Yang et al., 1999). A small number of studies have also used data acquired at multiple echo times to quantify the relaxation rate, R_2^*

* Corresponding author. Fax: +44 115 9515166.
E-mail address: Richard.Bowtell@nottingham.ac.uk (R. Bowtell).

1053-8119/$ – see front matter © 2009 Elsevier Inc. All rights reserved.
doi:10.1016/j.neuroimage.2009.05.015

and changes in this rate on activation, ΔR_2^*, (Gati et al., 1997; Yacoub et al., 2001). Such studies are valuable since they can shed light on the field dependence of the mechanism underlying BOLD contrast and also potentially provide measures that are more universal than the number of active voxels or average *t*-score, since the latter depends directly on the thresholding process used in the analysis and on the available signal to noise ratio. Previous studies in which ΔR_2^* was quantified have generally been performed in the visual cortex and also have been based on the use of surface RF coils for transmission and reception, and non-standard fMRI data acquisition methods, such as interleaved gradient echo EPI or gradient echo imaging, often applied to just a single slice.

The study described here compares the BOLD signal measured during execution of a simple motor task at three field strengths (1.5, 3 and 7 T), using MRI scanners with similar gradient and RF coils and a single-shot, multi-slice EPI acquisition. A motor task was chosen since it is a commonly used task which is easy to perform in a reproducible manner over a series of scanning sessions by controlling the intensity (tapping frequency) of the stimulus. Furthermore, the motor cortex is an attractive area to study since it is not greatly affected by susceptibility artefacts or B_1-inhomogeneity. fMRI was performed using a single-shot gradient echo EPI sequence at a resolution of 1×1 mm^2 in-plane and 3 mm slice thickness, reflecting the high spatial resolution that is currently being exploited in ultra-high field fMRI experiments (Speck et al., 2008). The relatively small voxel volume (3 mm^3) used here ensured that the intrinsic noise was larger than the physiological noise at all field strengths (Triantafyllou et al., 2005).

Data from multiple experiments run at different echo times were used to determine the variation in BOLD contrast with field strength in motor cortex, and the relative sensitivity of the BOLD signal to contributions from the tissue and venous compartments. Co-registration of the images acquired at the different field strengths allowed the relaxation rate, R_2^*, and its change on activation, ΔR_2^*, to be measured in the same, well-defined region at 1.5, 3 and 7 T.

Methods

Image acquisition

Six healthy volunteers (four female, two male, average age 33 ± 7 years) were recruited for these experiments. The study was approved by the local ethics committee and all subjects provided written consent. Subjects were scanned on Philips Achieva scanners (Philips Medical Systems, Best, NL) operating at field strengths of 1.5, 3 and 7 T. Standard quadrature, bird-cage T/R head coils were used at all field strengths for data acquisition.

fMRI data were acquired using a multi-slice, single-shot gradient echo (GE) EPI sequence, with outer volume suppression, on a 64×64 matrix with 1×1 mm^2 in-plane resolution and 3 mm slice thickness. Twelve contiguous, axial slices covering the right, primary motor cortex (MI) were scanned every 2 s using a flip angle of 80° and 80% coverage of *k*-space in the phase-encode direction. Outer volume suppression (OVS) (Pfeuffer et al., 2002) was used to prevent fold-over of signal in the phase-encode direction (anterior–posterior). This was achieved via excitation and subsequent crushing of the signal from two, 6-cm-wide rest slabs positioned posterior and anterior to the imaging volume, before excitation of each slice. The duration of the OVS module was approximately 11 ms. Comparison of data acquired from one subject with and without outer volume suppression showed that the addition of OVS caused a reduction of the temporal signal to noise ratio (measured from the ratio of the mean voxel intensity over ~250 voxels in grey matter to standard deviation with time) by less than 15% at all field strengths. This reduction is likely to be due to magnetisation transfer effects. At 7 T, the use of OVS increased the specific absorption rate (SAR) of the sequence by about 30%, however the SAR estimated by the scanner was still less than 1 W/kg.

fMRI experiments were performed at four echo times at each field strength. These were distributed around the expected optimum TE, and had values of 30, 50, 70 and 80 ms at 1.5 T; 22, 35, 50 and 65 ms at 3 T; and 18, 25, 34 and 43 ms at 7 T. The bandwidth per pixel in the phase-encode direction of the EPI acquisition was set to the maximum value allowed by the achievable gradient slew rates and amplitudes on each scanner. This gave values of 11.6, 14.8 and 18.2 Hz at 1.5, 3 and 7 T, reflecting the improved gradient system performance of the higher field scanners.

The following scanning procedure was followed at each of the three field strengths. At the start of the fMRI session, a volume of 40 contiguous, axial slices aligned parallel to the AC–PC line and spanning the entire brain volume with 3×3 mm^2 in-plane resolution and 3 mm slice thickness was acquired using a GE-EPI sequence (with echo times of 50, 35 and 25 ms at 1.5, 3 and 7 T, respectively). These 'whole head' volume data sets were used to localise the area of interest for the subsequent fMRI experiments. To simplify co-registration of the fMRI data, which had restricted volume coverage, to the 'whole head' data, a stack of 32 slices was also acquired with the same orientation and geometry as the fMRI data (64×64 matrix, 1-mm in-plane resolution and 3 mm slice thickness), but extending further in the inferior direction. This 'stack' data set was acquired with the same echo time as the 'whole head' images to facilitate later co-registration.

In addition to the EPI data, high-resolution T_1- and T_2^*-weighted images were acquired from each subject in separate scanning sessions to allow co-registration of functional images with anatomy and the identification of large veins, respectively. T_1-weighted data were acquired at 3 T using a standard MPRAGE sequence (Mugler and Brookeman, 1990) and an 8-element, head RF coil for signal reception. The MPRAGE images (TR = 14 ms, TI = 886 ms, TE = 3.8 ms) had a matrix size of $256\times256\times160$, isotropic 1 mm resolution, and were acquired with SENSE factor of 3 to reduce the acquisition time to 4.5 min. High-resolution, three dimensional, T_2^*-weighted images ($384\times258\times48$ matrix; $0.6\times0.6\times0.8$ mm^3 voxel size) were acquired from each subject at 7 T using a spoiled-FLASH sequence ($\alpha = 11°$; TR = 27 ms; TE = 15 ms) with a 7 minute acquisition time.

Paradigm

The functional paradigm consisted of a simple motor task, with an 8 s ON-period followed by a 20.25 s OFF period. This resulted in the paradigm being jittered with respect to the multi-slice image acquisition by 0.25 s per cycle. During the ON-period, subjects pressed a button using the thumb of their left hand. The motion amplitude was 7 mm and the rate of button pressing was approximately 3 Hz. A relatively long OFF period was used to provide adequate time for the haemodynamic response to return to baseline after each period of button pressing. Ten, seven or five cycles of the paradigm were executed at 1.5, 3 and 7 T, respectively for all four echo times. The higher number of cycles at lower field compensated in part for the expected reduction in BOLD contrast to noise ratio, and thus meant that there was sufficient statistical power to identify activated regions of interest (ROIs) on statistical parametric maps (SPMs) at all field strengths. However for subsequent quantitative analysis, which involved comparing the signal changes from ROIs defined from the SPMs, data from only the first 5 cycles of the paradigm were used at 1.5, 3 and 7 T to allow a fair comparison across fields and to minimize the effect of habituation. The order of acquisition of data across the four echo times was randomized across subjects at each field strength, so as to eliminate systematic adaptation effects. Scans at the different field strengths were acquired on different days, but for logistical reasons the 7 T data were acquired first, followed by the later acquisition of data at 1.5 and 3 T.

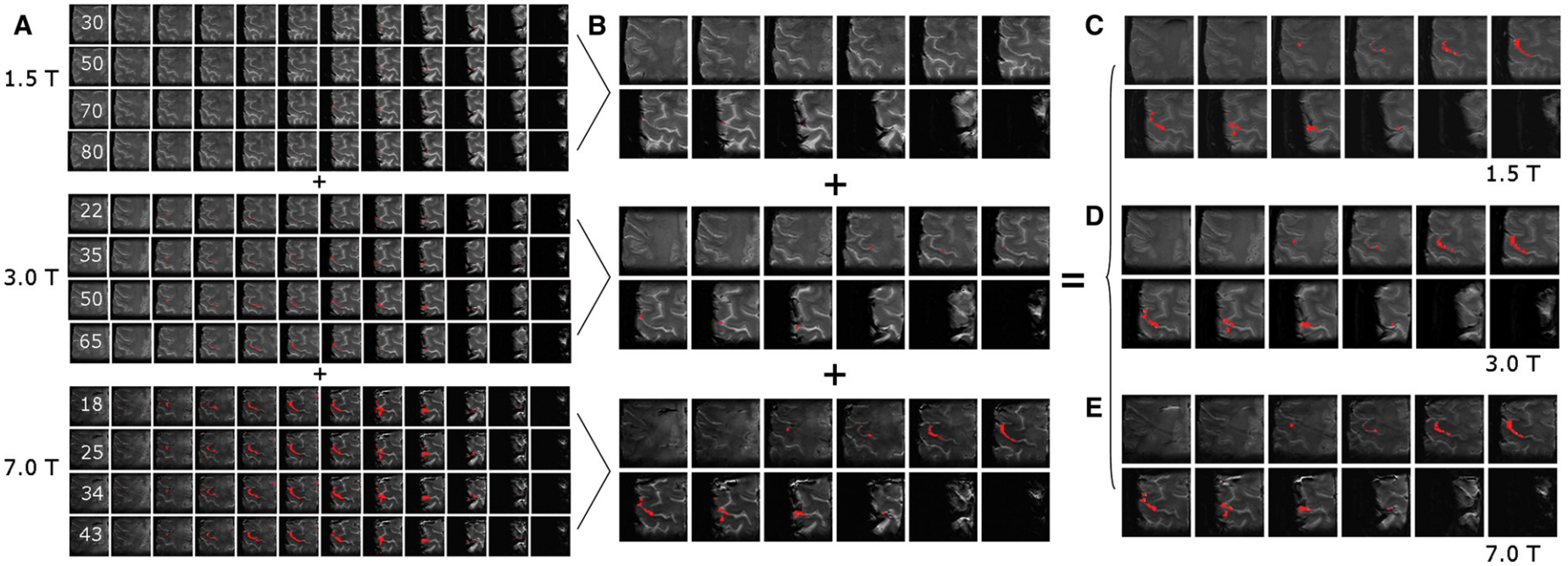

Fig. 1. Formation of the common ROI (subject 6). A: 12 SPMs formed from the different fMRI experiments. B: The logical AND is then used to form ROIs at 1.5, 3 and 7 T consisting of voxels which were classified as active at all echo times at the appropriate field strength. C: After transformation to the '1.5 T whole head' space, the common ROI is formed from the logical OR of the ROIs formed at the three field strengths. The common ROI is then transformed back to the individual field spaces: D 3 T, E: 7 T, and is shown here overlaid on the EPI data acquired at the second shortest echo time used at each field strength.

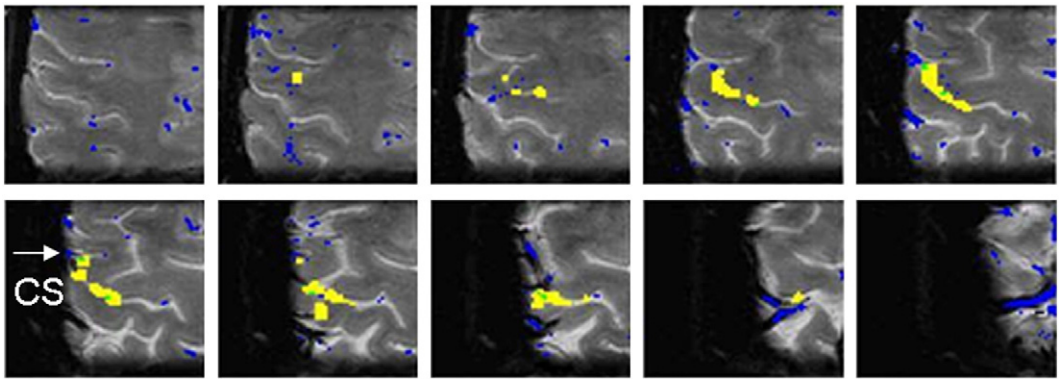

Fig. 2. Common ROI (yellow) and voxels classified as venous from the T_2^*-weighted images (blue) overlaid on 15 slices taken from the '1.5 T whole head' echo planar image (subject 6). Overlapping areas are shown in green. The central sulcus (CS) is indicated with an arrow.

Analysis

Initial image processing was performed using SPM2 (http://www.fil.ion.ucl.ac.uk/spm). Data series acquired at each echo time and field strength were corrected for slice timing effects and realigned. Next, for each field strength, the images acquired at the four different echo times were co-registered to the image data acquired at the second shortest echo time (50 ms at 1.5 T; 35 ms at 3 T; 25 ms at 7 T). We denote the frame of reference for these data as '1.5 T', '3 T' or '7 T' space. Spatial smoothing with a Gaussian kernel of 1.5 mm FWHM and high-pass temporal filtering with a cut-off period of 128 s were then applied. A general linear model was then formed with the BOLD signal change modelled as a box-car function (8 s high, 20.25 s low) convolved with the canonical haemodynamic response function (HRF). Motion parameters were included in the design matrix as covariates of no interest. Twelve statistical parametric maps were formed for each subject (corresponding to the four TE values at each of the three field strengths). All SPMs were thresholded at a family-wise error (FWE) corrected probability of 0.05, and a binary mask comprising voxels classified as active was also formed. The number of voxels in the binary mask within the motor cortex was measured for each of the twelve SPMs.

A common region of interest was then defined for each subject so as to allow measurement of the variation of BOLD signal change with echo time and field strength. To form this ROI, the data acquired at each of the field strengths were first co-registered (i.e. '1.5 T', '3 T' and '7 T' spaces were co-registered). Each of the twelve binary masks was then transformed to a standard space formed by the 1.5 T whole head data, via the following procedure. Using the FLIRT algorithm in FSL (Jenkinson and Smith, 2001), co-registration parameters were found which described the alignment of: (1) the fMRI data set with the second shortest echo to the 'stack' data acquired at the same field strength; (2) the 'stack' images to the 'whole head' images acquired at the same field strength; (3) the 'whole head' images obtained at 3 and 7 T to the 'whole head' images acquired at 1.5 T. The registration transforms identified in steps 1–3 were then concatenated to allow the transformation of all the binary masks to the '1.5 T whole head' space in a single step, thus limiting the amount of spatial smoothing introduced by the co-registration process. The transformed masks were re-thresholded to retain a constant number of active voxels following the transformation.

After transformation of all the binary masks to '1.5 T whole head' space, a binary mask (which we denote as the common ROI) was then formed for each subject by first applying the AND operation to the masks obtained at the four different echo times at each field strength, and then combining the three resulting masks for each field strength using the logical OR operation. The aim of this process was to identify voxels that were consistently activated in multiple experiments (via the AND operation), without strongly biasing the selection process to a particular field strength and allowing for some inaccuracy in co-registration of data sets acquired at the different field strengths (via the OR operation).

Having formed the binary mask in '1.5 T whole head' space it was then transformed to the 3 and 7 T field spaces by applying the concatenated transform in reverse and then re-thresholding to conserve the total number of voxels in the mask in each space. The average signal change, ΔS, fractional signal change, $\Delta S/S$, and t-value in the ROI were calculated for each echo time and field strength. ΔS

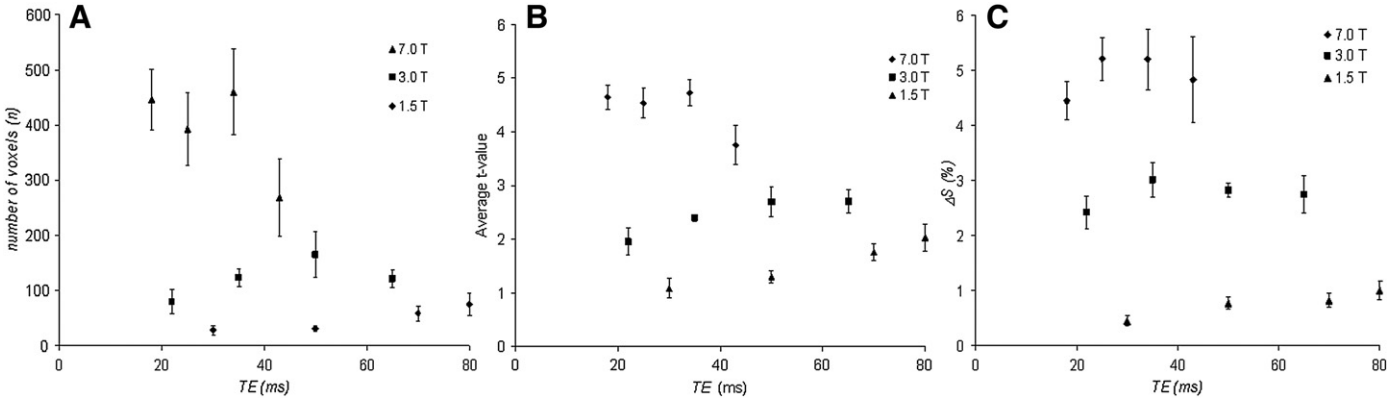

Fig. 3. BOLD parameters as a function of echo time. A: The number of active voxels (FWE $P_{corr}<0.05$) in the fMRI data sets averaged over all subjects is shown for each TE. B: The average t-value in the fMRI data sets averaged across the common ROI in all subjects is shown for each TE. C: Average BOLD signal change ΔS as a percentage of the signal recorded in the OFF period at the shortest echo time is plotted against TE. Error bars indicate the standard error.

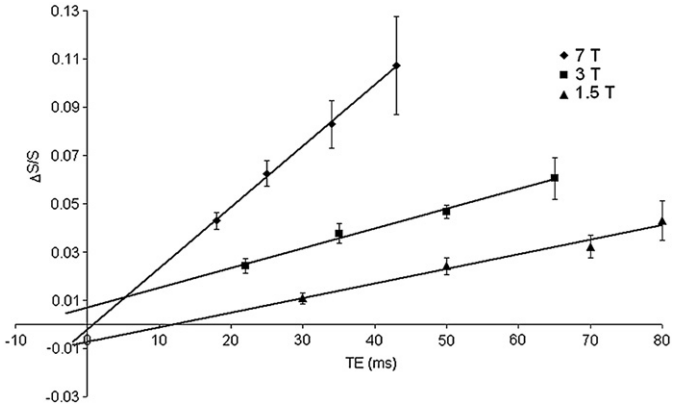

Fig. 4. Linear regression of $\Delta S/S$ versus TE for data averaged across all subjects at the three field strengths. $\Delta R_2{}^*$ values calculated from the gradients of the plots are displayed in Table 1.

was calculated from $(S_{ON} - S)$, where S_{ON} is the average of the four time-points spanning the peak of the HRF (approximately 6–12 s after the stimulus onset) and S is the average of four time-points in the OFF period (approximately 20–26 s after the stimulus onset). The signal change was calculated over the first five cycles of the paradigm. The t-value, given by $\Delta S / \sqrt{(\delta S_{ON})^2 + (\delta S)^2}$, where $(\delta S)^2$ represents the signal variance, was also calculated for each voxel in the ROI and averaged to provide a measure of the BOLD contrast to noise ratio. Since $\Delta S/S$ is expected to scale as $|\Delta R_2{}^* \times \mathrm{TE}|$ (Gati et al., 1997), a linear regression of $\Delta S/S$ against TE allowed evaluation of $\Delta R_2{}^*$ for the ROI. $R_2{}^*$ values in the ROI were also obtained at each field strength for each subject by un-weighted linear regression of $\ln(S_{OFF})$ against TE. Having calculated these values on an individual subject basis, these data were then combined to calculate the average over all subjects of $\Delta R_2{}^*$ and the ratio $\Delta R_2{}^*/R_2{}^*$ in the common ROIs at each field strength. In addition to the common ROI, we also formed a second, inclusion mask made up of voxels that were classed as active at any echo time or field strength. Use of this inclusion ROI allowed assessment of changes in $\Delta R_2{}^*$ and the ratio $\Delta R_2{}^*/R_2{}^*$ in a more extensive region of motor cortex. $\Delta R_2{}^*$ maps were also formed for each subject at each field strength by using a pixel-by-pixel linear regression of $\Delta S/S$ against TE.

A high-pass temporal filter with a cut-off frequency of 0.01 Hz was applied to the signal time-courses from the common ROI. For each subject the average high temporal resolution time-course of $\Delta S/S$ was obtained at each field strength by combining the time-points from the first five paradigm cycles using the known temporal offset of slice acquisitions from the start of the stimulus. These re-ordered time-courses were then averaged across all subjects. In order to provide an estimate of the onset time of the haemodynamic response at each of the three field strengths, the leading edge of the resulting HRFs was fitted to a linear function and the intercept of this line with the baseline was found (Gibson et al., 2005). The leading edge was identified from points on the rising curve with signal in the range of 10–90% of the maximum response, and the baseline was defined as the average signal intensity over the final 10 s period of all cycles.

To identify voxels in the common ROI which overlay large veins, the high-resolution, $T_2{}^*$-weighted images were also transformed to the '1.5 T whole head' space using FLIRT. Signal from outside the brain was first removed from these data using the brain extraction tool (BET) in FSL (Smith, 2002). Veins appear with low intensity in these images due to the short $T_2{}^*$ of venous blood at 7 T (Yacoub et al., 2001) and the relatively long echo time used. Before thresholding these data to form venous masks, it was necessary to eliminate large length-scale variation in image intensity due to RF inhomogeneity. This was accomplished by forming 3rd order polynomial fits to the images (on a slice-by-slice basis) and subtracting these from the original data to yield images in which veins appeared with low intensity on a uniform background. Using this information, voxels within the common ROI were divided into venous and tissue compartments, allowing histogram analysis of the BOLD signal change in large veins and tissue.

Results

The process by which the common ROIs were formed is illustrated for a representative subject (subject 6) in Fig. 1. Fig. 1A shows the binary masks formed by thresholding the SPMs obtained at each echo time at the three different field strengths. In each case the masks are overlaid on the mean of the EPI scans acquired with the second shortest echo time at the given field strength. These images clearly show the cortical anatomy at all field strengths and it can be seen that the size of the statistically significant active region increases considerably with field strength. The ROIs formed from the logical AND of the binary activation masks obtained at the four different echo times at each field strength are shown in Fig. 1B. The common ROI formed by applying the OR operation to the masks in Fig. 1B is shown in Fig. 1C, overlaid on the mean of the fMRI data set acquired with TE = 50 ms at 1.5 T. It can be seen that the activation is found along the cortical strip of the central sulcus and pre-central gyrus, as expected for movement of the thumb. This is also overlaid on the fMRI data set acquired with TE = 50 ms at 1.5 T. Fig. 1D shows the common ROI transformed into the 3 T space and overlaid on the data acquired at the second shortest echo time. Fig. 1E similarly shows the common ROI overlaid on the 7 T data with TE = 25 ms. The correspondence of the ROI with the anatomical features evident in the echo planar images acquired at the three different field strengths provides an indication of the efficacy of the co-registration process.

Fig. 2 shows the overlap (green) of the common ROI (yellow) with areas identified as corresponding to large veins in the high-resolution $T_2{}^*$-weighted images (blue) acquired at 7 T for subject 6. Only a relatively small fraction of the voxels within the common ROI corresponds to large veins for this subject, but averaged over all subjects the fraction of voxels in the ROI that were classified as venous was 25%.

Fig. 3A shows the number of active voxels (FWE $P_{corr} < 0.05$) averaged across the 6 subjects plotted against echo time at 1.5, 3 and 7 T. The variation with echo time of the average t-value calculated over the common ROI is shown in Fig. 3B for each field strength. Fig. 3C plots the signal change in the common ROI averaged across subjects against echo time. For these data, the signal changes were scaled by the average signal measured from the common ROI in the OFF period using the shortest echo time at each field strength before averaging over subjects.

Fig. 4 shows the average fractional signal change ($\Delta S/S$) across the common ROI in all subjects at each echo time. Table 1 shows the gradient, intercept and R^2 value of the linear regression of $\Delta S/S$ values averaged over all subjects versus TE. These average $\Delta S/S$ data showed a linear relationship with TE, with an intercept that was not significantly different from zero (Table 1). $\Delta R_2{}^*$ values were therefore subsequently fitted on a per subject basis assuming a zero intercept to reduce fitting errors.

Fig. 5A shows $\Delta R_2{}^*$ maps obtained for subject 6 by applying a linear regression assuming zero intercept to the image data on a pixel-by-pixel basis. These are overlaid on the mean of the EPI scans with

Table 1
Results of linear fits to plots of $\Delta S/S$ averaged over all subjects versus TE.

	1.5 T	3.0 T	7.0 T
Gradient (s^{-1})	0.6 ± 0.3	0.8 ± 0.2	2.6 ± 0.3
Intercept	-0.01 ± 0.02	0.01 ± 0.01	0.00 ± 0.01
R^2 value	0.975	0.991	0.998

The value of $\Delta R_2{}^*$ in the common ROI is given by the gradient of the fit.

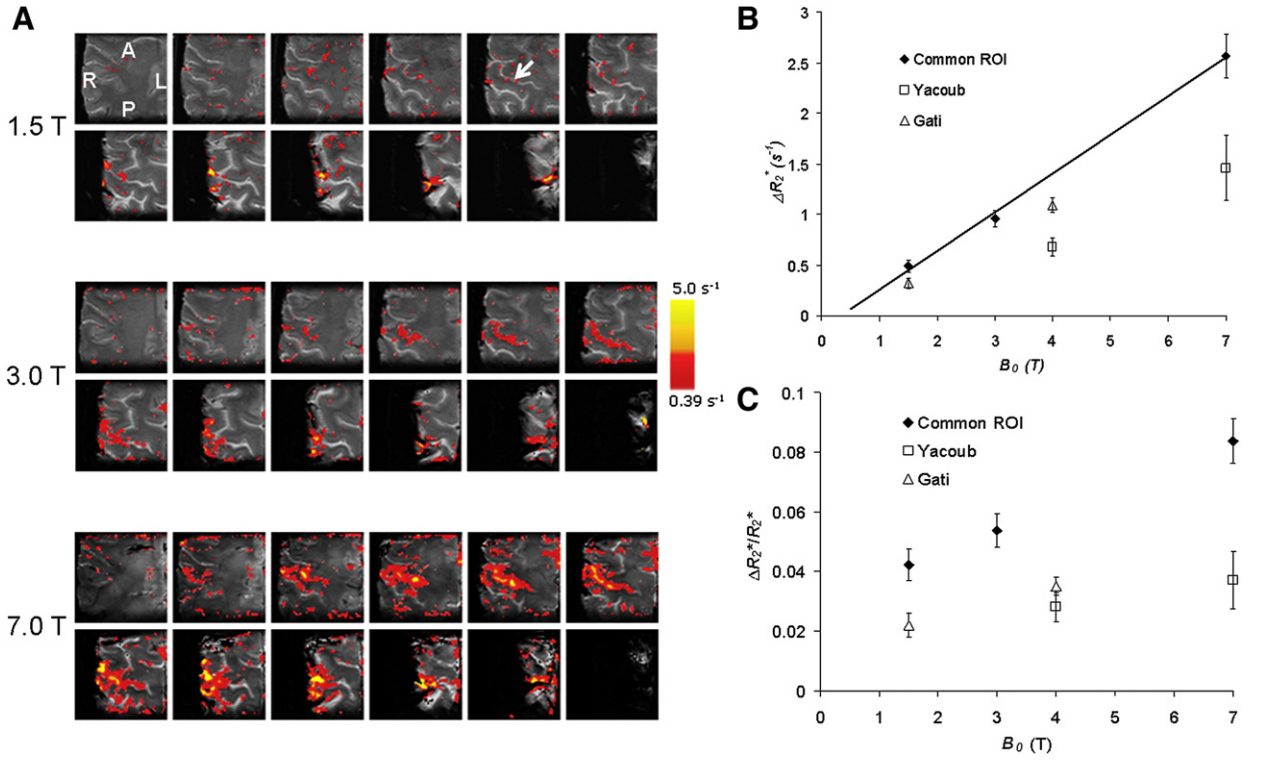

Fig. 5. A: ΔR_2^* maps calculated for a representative subject (subject 6) at 1.5, 3 and 7 T. The ΔR_2^* data are shown overlaid on the mean of the echo planar data acquired using the second shortest echo time at each field strength. The arrow indicates the central sulcus. All maps are displayed with a threshold set to $\Delta R_2^* > 0.39\ s^{-1}$. The colour-bar indicates the range of ΔR_2^*. B: ΔR_2^* averaged over all subjects against field strength, a linear regression was applied to the data and gave a gradient of $0.38\ s^{-1}\,T^{-1}$ with an intercept of $-0.13\ s^{-1}$. Literature data (Gati et al., 1997; Yacoub et al., 2001) is also shown. C: The ratio $\Delta R_2^*/R_2^*$ averaged over all subjects is plotted against field strength together with literature data. Error bars indicate the standard error.

the second shortest TE. The threshold for all ΔR_2^* maps has been set to $0.39\ s^{-1}$, which was the average ΔR_2^* value measured in the common ROI at 1.5 T. The total number of voxels and the average values of ΔR_2^* and R_2^* calculated for the common ROI for each subject are shown in Table 2. The variation with field strength of the average value across subjects of ΔR_2^* the common ROI is shown in Fig. 5B, along with tissue ΔR_2^* values measured in previous studies of BOLD signal changes in visual cortex by Gati et al. (1997) and Yacoub et al. (2001). A linear regression with field strength is shown for our data and this yields $R^2 = 0.997$. Fig. 5C plots $\Delta R_2^*/R_2^*$ averaged over all subjects, against field strength. Literature data (Gati et al., 1997; Yacoub et al., 2001) are again included for comparison.

Fig. 6 shows histograms of the ΔR_2^* values measured within the common ROI separated into venous and tissue compartments (classification based on the high-resolution T_2^*-weighted data). In these data, which were pooled across subjects, 168 voxels were classified as venous and 589 as tissue. The mean and standard deviation of ΔR_2^* in the two compartments calculated across the data from the six subjects at each field strength are detailed in Table 3.

Fig. 7A shows the variation of the fractional change in the average signal from the common ROI (including both venous and tissue voxels) in one representative subject during the first 5 cycles of the experiment carried out at the second shortest echo time at the three different field strengths (50, 35, 25 ms at 1.5, 3 and 7 T, respectively). Time-courses have been normalised to the mean of the signal in the OFF period. Fig. 7B shows similar plots formed by averaging over the data from all six subjects. A linear fit to the leading edge of the cycle-average of the HRFs shown in Fig. 7B is plotted in Fig. 7C; the intersection of this fit with the baseline occurred at times of 3.6 ± 0.4, 2.8 ± 0.3 and 2.5 ± 0.2 s following stimulus onset at 1.5, 3 and 7 T respectively.

Discussion

This work adds to previous studies of the field strength dependence of BOLD signal characteristics, through its: (i) focus on motor rather than visual cortex; (ii) use of single-shot, multi-slice, gradient echo EPI for data acquisition; (iii) co-registration of images

Table 2
Number of voxels in the common ROI, along with ΔR_2^* and R_2^* values.

Subject	Number of voxels	1.5 T		3.0 T		7.0 T	
		ΔR_2^* (s^{-1})	R_2^* (s^{-1})	ΔR_2^* (s^{-1})	R_2^* (s^{-1})	ΔR_2^* (s^{-1})	R_2^* (s^{-1})
1	69	0.40	10.7	0.89	18.3	1.91	31.8
2	85	0.52	11.5	1.06	18.4	2.72	35.3
3	238	0.53	12.6	0.75	18.0	2.30	29.6
4	74	0.35	12.0	0.89	19.2	2.29	28.9
5	74	0.76	11.5	1.32	16.6	3.51	30.9
6	217	0.39	11.5	0.86	17.8	2.71	28.4
Mean ± standard error	108 ± 30	0.51 ± 0.06	11.6 ± 0.3	0.98 ± 0.08	18.1 ± 0.4	2.55 ± 0.22	30.8 ± 1.0

ΔR_2^* was obtained at each field strength from a linear fit to the fractional change in the signal from the ROI assuming a zero intercept. Mean values of all parameters ($\pm$ standard error) across subjects are also listed.

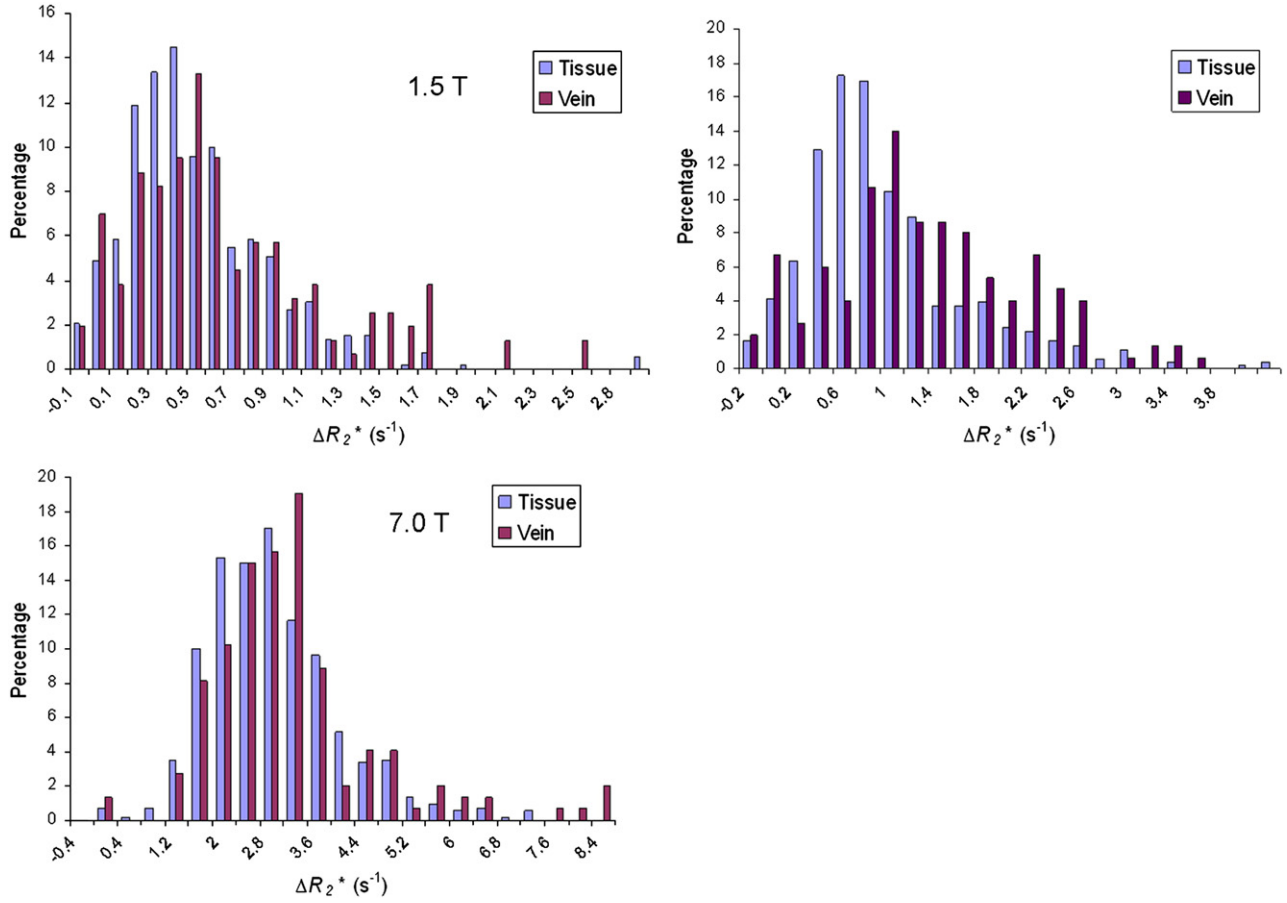

Fig. 6. Histograms displaying the distribution of ΔR_2^* values found over voxels in venous and tissue compartments at 1.5, 3 and 7 T.

acquired at different field strengths to allow assessment of the BOLD signal changes in the same region of motor cortex at each field strength.

The differences in the experimental method used in this study compared with previous work are relevant, since use of different regions of the brain, imaging sequences, RF coil types and spatial resolutions will affect the signal to noise ratio of the measurements. The effect of these differences would mainly be expected to be manifested in changes in the measures of the BOLD response that are directly sensitive to the signal to noise ratio (number of active pixels and average *t*-score). The most important difference from previous work is the use of a multi-slice data acquisition, which allowed us to co-register the data acquired at the three fields and thus to measure the signal changes in the same, well-defined ROI at 1.5, 3 and 7 T. The co-registration also allowed the ROI to be based on combination of the active areas identified at all three field strengths. Study of motor rather than visual cortex may also alter the results due to differences in vascularisation (Marcar et al., 2004). Baseline R_2^* differences between different cortical regions have previously been identified (Bartha et al., 2002; Zhou et al., 2001).

In previous work carried out across a lower range of field strengths (1.5, 3 and 4 T), Gati et al. (1997) used a spoiled gradient echo acquisition of single-slice data to show that the BOLD signal change in visual cortex was larger in veins than tissue, but that the signal change in tissue increased more rapidly with field strength. Working at 4 and 7 T in the visual cortex using single-shot EPI, Duong et al. (2003a), showed that at these field strengths the gradient echo BOLD signal was dominated by tissue. Yacoub et al. (2001), also working at 4 and 7 T in the visual cortex, but using single-slice segmented EPI, found that the sensitivity and spatial specificity of the BOLD effect increased with field strength. Yang et al. used 3D, interleaved, spiral EPI to compare the BOLD responses to a motor task at 1.5 and 4 T and showed a significant increase in the number and average *t*-score of activated voxels at the higher field. Fera et al. (2004) working at 1.5 and 3 T in the motor cortex using single-shot gradient echo EPI, showed a lower than expected increase in SNR with field strength which they attributed to the effect of physiological noise. Krasnow et al. (2003) extended previous studies by comparing the volume of activation and mean *Z*-scores produced in a range of brain areas at 1.5 and 3 T during execution of tasks involving perceptual, cognitive, and affective processing. The significant increases in these measures that they identified at 3 T showed that functional imaging of pre-frontal and other association cortices benefits from the use of higher field. There have also been a number of other studies that have considered the variation in the sensitivity of spin echo BOLD effects across field strength (Duong et al., 2002, 2004; Hulvershorn et al., 2005; Schaefer et al., 2008; Yacoub et al., 2003, 2005, 2007).

An increased BOLD contrast to noise ratio allows fMRI to be performed at higher spatial resolution, which has the potential advantage of reduced signal drop-out due to magnetic field inhomogeneities (Weiskopf et al., 2007) and longer baseline T_2^* (Speck et al., 2008). At high resolution the effect of intrinsic noise also dominates that of physiological noise so that the full benefit of the increased

Table 3
Variation of average ΔR_2^* over subjects with field strength in venous and tissue compartments.

ΔR_2^*/field	1.5 T	3.0 T	7.0 T
Venous ΔR_2^* (s^{-1})	0.76 ± 0.22	0.96 ± 0.24	2.39 ± 0.49
Tissue ΔR_2^* (s^{-1})	0.49 ± 0.06	0.97 ± 0.08	2.55 ± 0.21

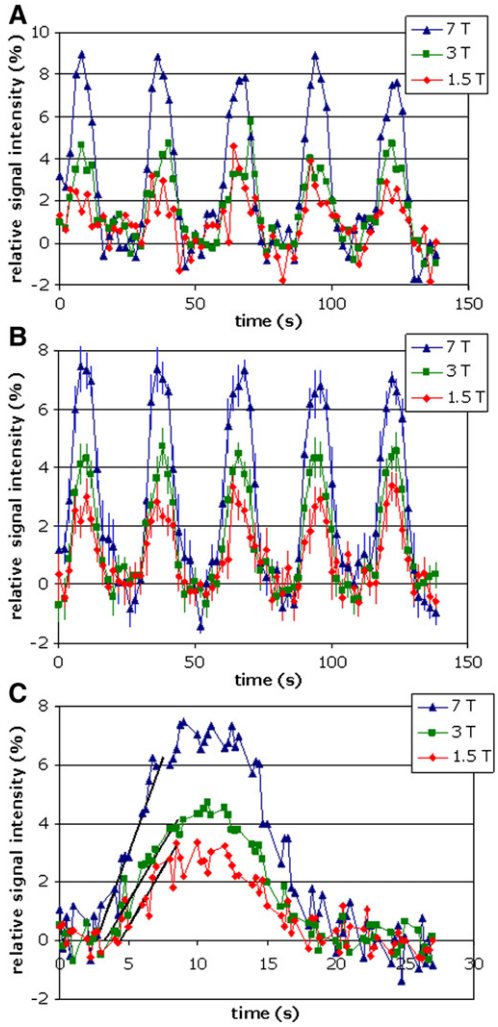

Fig. 7. A: Time-courses for a representative subject (subject 6) at the optimum echo time per field strength. (70, 35, 25 ms for 1.5, 3 and 7 T) B: Time-courses at optimum TE, averaged over all subjects. C: Time-course as in B ordered to the temporal offset from the start of the stimulus. All graphs are normalised to the mean signal in the OFF period. A linear fit is applied to the leading edge of the HRF. The start of the HRF as determined by the fit was 3.6 ± 0.4, 2.8 ± 0.3 and 2.5 ± 0.2 s after the start of the stimulus at 1.5, 3 and 7 T, respectively.

BOLD contrast at high field can be realised (Triantafyllou et al., 2005). In the study described here, functional sensitivity was compared across three different field strengths at a relatively high spatial resolution ($1 \times 1 \times 3$ mm^3). Such high spatial resolution is now standard for fMRI acquisition at 7 T (Speck et al., 2008). In our study, OVS had to be used to obtain this resolution while avoiding fold-over artefacts. At high field, errors in shimming can lead to distortion of the suppression bands used in OVS, but this effect was not significant in the brain areas studied in these experiments, as can be seen from Fig. 1. Parallel imaging (Pruessmann et al., 1999) could be used to increase the field of view in the phase-encode direction without compromising the bandwidth per pixel, but unfortunately at the time of this study only a single RF channel was available for signal reception on our 7 T scanner.

The voxel volume used in this study is similar to that described by Yacoub et al. (2001) who used segmented EPI to produce images with a voxel size of $0.78 \times 0.78 \times 5$ mm^3, but smaller than that of Gati et al. (1997) who used a spoiled gradient echo sequence with a resolution of $1.25 \times 1.25 \times 5$ mm^3, Duong et al. (2003a) who used single-shot GE- and SE-EPI with a resolution of $3.1 \times 3.1 \times 10$ mm^3, and Fera et al. (2004) who used single-shot EPI with a resolution of $3.75 \times 3.75 \times 4$ mm^3. The temporal resolution used in our study was 2 s which is typical for fMRI experiments, but higher than that used in the previous studies listed above.

Previous studies in which changes in R_2^* on activation have been quantified have used a variety of methods for identifying the region of interest that was interrogated at the different field strengths. Gati et al. (1997) used different ROIs at each field strength, based on pixels which showed activation above a common threshold and which lay in the cortical strip, but did not overlie large veins. Duong et al. (2003a) used a region based on voxels that were classified as active in a single data set acquired at each field strength. With both these methods it is possible that signals from different brain regions were considered at the different echo times and/or field strengths, potentially causing the results to be dominated by areas that have high BOLD sensitivity under different conditions. Yacoub et al. (2001) aimed to interrogate the same tissue and venous regions of interest at 4 and 7 T. However this process relied on selecting an identical sagittal slice for image acquisition at the two field strengths and then using anatomical landmarks to site the ROIs. Such a process is subject to some error in positioning, so that slightly different regions may have been sampled at the two field strengths. In addition the tissue region, which was defined based on an activation map, appears to encompass a whole sulcus and may also therefore have included a significant contribution from cerebrospinal fluid (CSF).

In contrast to previous work, in this study we measured the variation of BOLD signal change with echo time in the same region of the motor cortex at the three different field strengths in each subject. This was made possible by co-registration of multi-slice data acquired at the different field strengths. We chose not to use an anatomically-defined region of interest since this could have led to "partial voluming" with inactive areas including contributions from CSF and white matter. We aimed to generate regions of interest that showed consistent activation by forming the common ROI from the logical AND of the voxels that were active across all echo times for a given field strength, but then calculated the logical OR between field strengths to account for any small registration errors and to avoid biasing the selection too strongly towards one field strength. Figs. 1C–E provide visual evidence of the accuracy of co-registration across field strengths.

To help ensure that there was adequate power to detect activation at the lower fields a larger number of cycles were also used in the analysis when forming the binary mask. Co-registration of the functional data with high-resolution, T_2^*-weighted images acquired at 7 T indicated that on average across all subjects 25% of active voxels overlaid large veins (Fig. 2).

In our study, baseline R_2^* increased with field strength as expected (Table 2) and the values were also reasonably consistent with those previously described in the literature (Fera et al., 2004; Gati et al., 1997; Peters et al., 2007; Yacoub et al., 2001), although some differences might be expected due to differences in the shimming methods, voxel size, region of interest definition, and anatomical regions studied. Other previous studies have often used larger voxels or less precisely defined regions of interest which will have caused partial voluming with CSF, potentially leading to an under-estimation of R_2^*. There are also some known variations in T_2^* across the cortex that will have contributed to these differences; in particular we studied the motor area whereas other work up to 7 T studied the visual area which is thought to have a shorter T_2^* (Bartha et al., 2002; Zhou et al., 2001).

The number of activated voxels, the average *t*-score, and signal change (Fig. 3) within the common ROI all peaked at an echo time that corresponded to the value of T_2^* measured at each field strength (Table 2). Similar results have previously been reported under different experimental conditions as outlined above (Fera et al., 2004; Gati et al., 1997; Yacoub et al., 2001). Measures of BOLD contrast to noise ratio, such as the number of activated voxels and

average t-score, are only expected to be maximised when TE = T_2^* if the noise is independent of echo time, as is the case when the intrinsic rather than physiological noise dominates. The behaviour displayed in Figs 3A and B thus indicates the dominance of the intrinsic noise, as would be expected to be the case in data acquired at 1.5, 3 and 7 T at $1\times1\times3$ mm^3 resolution using TR = 2 s, based on the work of Triantafyllou et al. (2005). Signal variation due to direct effects of respiration (van Gelderen et al., 2007) would be expected to be of greater severity in more inferior brain regions and variability due to task performance would clearly be more significant if more complex tasks were employed.

The plot of $\Delta S/S$ against TE averaged over the region of interest (Fig. 4) showed a linear relationship with an intercept that was not significantly different to zero (Table 1), suggesting that the signal changes were dominated by BOLD R_2^* changes rather than in-flow effects at all field strengths. This finding also indicates that the effect of the BOLD R_2^* increase on the point spread function which can cause signal changes that are independent of echo time (Schaefer et al., 2008) was not significant for these data.

Considering the ΔR_2^* maps, large changes in R_2^* were observed in areas of the motor cortex that corresponded to the active areas in the SPMs (Fig. 5A). Only small areas with $\Delta R_2^* \geq 0.39$ s^{-1} were found at 1.5 T and these showed significant overlap with veins. Larger areas with $\Delta R_2^* \geq 0.39$ s^{-1} were found in the 3 and 7 T data and these extended along a thin strip following the central sulcus, spanning the region where the cortical representation of the thumb is expected. At 7 T, very high ΔR_2^* values (≥ 5 s^{-1}) were found in some areas.

Fig. 5B shows that the ΔR_2^* value formed by averaging over subjects varies linearly when plotted against field strength ($R^2 = 0.9975$) and that the resulting plot has an approximately zero intercept. This implies that the measured signal changes are dominated by static dephasing effects around vessels (Gati et al., 1997), rather than by the effect of diffusion through extravascular gradients which would generate a dependence on field strength tending to a quadratic form (Kennan et al., 1991). In these circumstances, R_2^* varies as $\frac{4}{3}\pi\gamma B_0\chi$ (Yablonskiy and Haacke, 1994) (where V is the blood volume and χ is the blood-tissue susceptibility difference) and ΔR_2^* is thus expected to vary proportionally with field strength, B_0, as can be observed in Fig. 5B. Assuming a resting venous blood volume of 3% (Duong et al., 2002), a fractional change in venous blood volume of 28% (Pears et al., 2003), a resting venous oxygenation (Y_{rest}) of 0.6, a haematocrit of 0.4, a susceptibility difference between deoxygenated and oxygenated blood of 1.8×10^{-7} cgs units (Weisskoff and Kiihne, 1992) and hence a resting venous susceptibility of 3×10^{-8} cgs units, then using the gradient of Fig. 5B we measure a change in venous blood susceptibility on activation of 1.5×10^{-8} corresponding to an activated venous oxygenation (Y_{act}) of 0.8. This would correspond to a decrease in oxygen extraction fraction on activation of just less than 50% which is in reasonable agreement with the literature (Gibson et al., 2005).

$\Delta R_2^*/R_2^*$ was found to increase with field strength (Fig. 5C), implying that ΔR_2^* increases more significantly than R_2^* with increasing B_0. This is consistent with the findings of previous studies in the visual cortex (Gati et al., 1997; Yacoub et al., 2001) and with the observation that the BOLD percentage change in signal produced at the optimal echo time is higher at high field. The values of ΔR_2^* and $\Delta R_2^*/R_2^*$ measured in motor cortex in this study and their rate of change with B_0 are higher than those observed previously in visual cortex (Gati et al., 1997; Yacoub et al., 2001). This most probably results from the use of a tighter, functionally derived region of interest in our study. In support of this statement, we note that a separate analysis of the data using the looser mask of voxels corresponding to those that were classified as active at any echo time or field strength gave values of ΔR_2^* (0.28 ± 0.02 s^{-1} at 1.5 T; 0.54 ± 0.03 s^{-1} at 3 T; 1.28 ± 0.08 s^{-1} at 7 T) and $\Delta R_2^*/R_2^*$ (0.022 ± 0.001 at 1.5 T; 0.028 ± 0.002 at 3 T; 0.035 ± 0.002 at 7 T) that were similar to the literature results (Gati et al., 1997; Yacoub et al., 2001).

Physiological noise can reduce the gains in BOLD contrast to noise ratio at ultra-high field that Fig. 5B predicts. Returning to Fig. 3B, it can be seen that the average t-value in the ROI at the optimum echo time increased with field strength, although not as fast as the change in R_2^*. The increase in t-value between 3 and 7 T was relatively larger than that between 1.5 and 3 T, suggesting that at the high spatial resolution used here ($1\times1\times3$ mm^3) 7 T provided increased detection power and that the contrast to noise ratio is not dominated by the effect of physiological noise. A clearer demonstration of increased detection power due to increased BOLD sensitivity and signal to noise ratio at 7 T was provided by the increase in the number of activated voxels (Fig. 3A). The peak value of this number increases by nearly a factor of three between 3 and 7 T. This occurs despite the use of a reduced bandwidth at the lower field strength, which will have acted to provide a relative increase in the signal to noise ratio at 3 T (Zou et al., 2005).

Fig. 6 shows the normalised distribution of ΔR_2^* values at the three different field strengths over the voxels within the common ROI which were classified as corresponding to veins or tissue. At 7 T, all voxels in the ROI showed a positive change in ΔR_2^*, which was not the case at lower fields, indicating that at 7 T it is possible to detect activated areas whose signal changes fall within the noise at lower fields. The distributions of ΔR_2^* values in the voxels classified as overlying large veins (based on the high-resolution T_2^*-weighted images) do not show strong differences from those measured from tissue, although at all field strengths the venous data shows some evidence of a larger tail in the distribution at high ΔR_2^* values. When paired t-tests were carried out on the ΔR_2^* values measured in the two compartments across subjects (using the data summarised in Table 3), no significant difference was found at any field strength, although at 1.5 T the difference approached significance ($p = 0.1$). In previous work, the BOLD-related R_2^* changes in the venous compartment were identified as being larger than those in tissue at 0.5, 1.5 and 4 T (Gati et al., 1997; Yacoub et al., 2001), although similar values of ΔR_2^* were measured in the two compartments at 7 T (Yacoub et al., 2001). The discrepancy with the present study may be a consequence of the larger tissue ΔR_2^* values measured. However in addition, the longer minimum echo times and smaller image bandwidths used in our study compared with the previous work (Gati et al., 1997; Yacoub et al., 2001), will have given rise to a relative attenuation of the venous signal due its short T_2^* and a broader point spread function for the venous compartment. Together these effects are likely to have resulted in contamination of the signal from small veins with the significantly larger signal from surrounding tissue.

Individual trials in this block paradigm could easily be detected in the time-course data from the ROIs for these high-resolution images at all field strengths (Figs. 7A and B). The fits to the leading edge of the HRF indicated that the onset time (3.6 ± 0.4, 2.8 ± 0.3 and 2.5 ± 0.2 s after the start of the stimulus at 1.5, 3 and 7 T, respectively) was earlier at 7 T than 3 T or 1.5 T (Fig. 7C), although only the largest difference, between the onset times measured at 1.5 and 7 T, was significant ($p = 0.07$). It would be expected that the onset time would be later for contributions to the signal from draining veins compared with signal from tissue, since BOLD signal changes in response to increased neuronal activity occur initially in the microvasculature and then propagate into the venous compartment (de Zwart et al., 2005; Hulvershorn et al., 2005). The delay in onset found at 7 T compared with the lower field strengths would be consistent with a suppression of the delayed BOLD contribution from the venous compartment at higher field strengths (Duong et al., 2003a). The 1.1 s difference in onset times measured at 1.5 and 7 T is comparable in size to the 0.7 s reduction in time to peak found when comparing spin and gradient echo data (Hulvershorn et al., 2005) and is consistent with the findings of de Zwart et al. (de Zwart et al., 2005) who simulated the red blood cell transit through the post-capillary vasculature. The reduced sensitivity to the venous compartment that these data imply would clearly be beneficial for accurate measurement of the timing of

haemodynamic responses across different brain regions, since it is likely to reduce the variability in the width and time to peak of the BOLD response.

Acknowledgments

This work was funded by MRC/EPSRC grant number G9900259. The 7 T facility was funded by a JIF grant from the Wellcome Trust.

References

Bartha, R., Michaeli, S., Merkle, H., Adriany, G., Andersen, P., Chen, W., Ugurbil, K., Garwood, M., 2002. In vivo 1H2O $T2^{+}$ measurement in the human occipital lobe at 4 T and 7 T by Carr–Purcell MRI: detection of microscopic susceptibility contrast. Magn. Reson. Med. 47, 742–750.

Bodurka, J., Ye, F., Petridou, N., Murphy, K., Bandettini, P.A., 2007. Mapping the MRI voxel volume in which thermal noise matches physiological noise—implications for fMRI. Neuroimage 34, 542–549.

de Zwart, J.A., Silva, A.C., van Gelderen, P., Kellman, P., Fukunaga, M., Chu, R., Koretsky, A.P., Frank, J.A., Duyn, J.H., 2005. Temporal dynamics of the BOLD fMRI impulse response. Neuroimage 24, 667–677.

Duong, T.Q., Yacoub, E., Adriany, G., Hu, X.P., Ugurbil, K., Vaughan, J.T., Merkle, H., Kim, S. G., 2002. High-resolution, spin-echo BOLD, and CBF AM at 4 and 7 T. Magn. Reson. Med. 48, 589–593.

Duong, T.Q., Yacoub, E., Adriany, G., Hu, X., Ugurbil, K., Kim, S.G., 2003a. Microvascular BOLD contribution at 4 and 7 T in the human brain: gradient-echo and spin-echo fMRI with suppression of blood effects. Magn. Reson. Med. 49, 1019–1027.

Duong, T.Q., Yacoub, E., Adriany, G., Hu, X.P., Ugurbil, K., Kim, S.G., 2003b. Microvascular BOLD contribution at 4 and 7 T in the human brain: gradient-echo and spin-echo fMRI with suppression of blood effects. Magn. Reson. Med. 49, 1019–1027.

Duong, T.Q., Yacoub, E., Adriany, G., Hu, X.P., Andersen, P., Vaughan, J.T., Ugurbil, K., Kim, S.G., 2004. Spatial specificity of high-resolution, spin-echo BOLD, and CBF fMRI at 7 T. Magn. Reson. Med. 51, 646–647.

Fera, F., Yongbi, M.N., van Gelderen, P., Frank, J.A., Mattay, V.S., Duyn, J.H., 2004. EPI-BOLD fMRI of human motor cortex at 1.5 T and 3.0 T: sensitivity dependence on echo time and acquisition bandwidth. J. Magn. Reson. Imaging 19, 19–26.

Gati, J.S., Menon, R.S., Ugurbil, K., Rutt, B.K., 1997. Experimental determination of the BOLD field strength dependence in vessels and tissue. Magn. Reson. Med. 38, 296–302.

Gibson, A.M., Brookes, M.J., Kim, S.S., Francis, S.T., Morris, P.G., 2005. A new quantitative analysis of significant timing differences between externally cued and self-initiated motor tasks in an fMRI study. Solid State Nucl. Magn. Reson. 28, 258–265.

Hulvershorn, J., Bloy, L., Gualtieri, E.E., Leigh, J.S., Elliott, M.A., 2005. Spatial sensitivity and temporal response of spin echo and gradient echo bold contrast at 3 T using peak hemodynamic activation time. Neuroimage 24, 216–223.

Jenkinson, M., Smith, S., 2001. A global optimisation method for robust affine registration of brain images. Med. Image Anal. 5, 143–156.

Kennan, R.P., Zhong, J., Gore, J.C., 1991. On the relative importance of paramagnetic relaxation and diffusion-mediated susceptibility losses in tissues. Magn. Reson. Med. 22, 197–203 discussion 213–195.

Krasnow, B., Tamm, L., Greicius, M.D., Yang, T.T., Glover, G.H., Reiss, A.L., Menon, V., 2003. Comparison of fMRI activation at 3 and 1.5 T during perceptual, cognitive, and affective processing. Neuroimage 18, 813–826.

Marcar, V.L., Straessle, A., Girard, F., Loenneker, T., Martin, E., 2004. When more means less: a paradox BOLD response in human visual cortex. Magn. Reson. Imaging 22, 441–450.

Mugler, J.P., Brookeman, J.R., 1990. 3-Dimensional magnetization-prepared rapid gradient-echo imaging (3dmp-Rage). Magn. Reson. Med. 15, 152–157.

Ogawa, S., Menon, R.S., Kim, S.G., Ugurbil, K., 1998. On the characteristics of functional magnetic resonance imaging of the brain. Annu. Rev. Biophys. Biomol. Struct. 27, 447–474.

Pears, J.A., Francis, S.T., Butterworth, S.E., Bowtell, R.W., Gowland, P.A., 2003. Investigating the BOLD effect during infusion of Gd-DTPA using rapid T2* mapping. Magn. Reson. Med. 49, 61–70.

Peters, A.M., Brookes, M.J., Hoogenraad, F.G., Gowland, P.A., Francis, S.T., Morris, P.G., Bowtell, R., 2007. T-2* measurements in human brain at 1.5, 3 and 7 T. Magn. Reson. Imaging 25, 748–753.

Pfeuffer, J., van de Moortele, P.F., Yacoub, E., Shmuel, A., Adriany, G., Andersen, P., Merkle, H., Garwood, M., Ugurbil, K., Hu, X.P., 2002. Zoomed functional imaging in the human brain at 7 Tesla with simultaneous high spatial and high temporal resolution. Neuroimage 17, 272–286.

Pruessmann, K.P., Weiger, M., Scheidegger, M.B., Boesiger, P., 1999. SENSE: sensitivity encoding for fast MRI. Magn. Reson. Med. 42, 952–962.

Schaefer, A., van der Zwaag, W., Francis, S.T., Head, K.E., Gowland, P.A., Bowtell, R.W., 2008. High resolution SE-fMRI in humans at 3 and 7 T using a motor task. Magn. Reson. Mater. Phys. Biol. Med. 21, 113–120.

Smith, S.M., 2002. Fast robust automated brain extraction. Hum. Brain Mapp. 17, 143–155.

Speck, O., Stadler, J., Zaitsev, M., 2008. High resolution single-shot EPI at 7 T. Magn. Reson. Mater. Phys. Biol. Med. 21, 73–86.

Triantafyllou, C., Hoge, R.D., Krueger, G., Wiggins, C.J., Potthast, A., Wiggins, G.C., Wald, L.L., 2005. Comparison of physiological noise at 1.5 T, 3 T and 7 T and optimization of fMRI acquisition parameters. Neuroimage 26, 243–250.

Turner, R., Jezzard, P., Wen, H., Kwong, K.K., Le Bihan, D., Zeffiro, T., Balaban, R.S., 1993. Functional mapping of the human visual cortex at 4 and 1.5 Tesla using deoxygenation contrast EPI. Magn. Reson. Med. 29, 277–279.

van Gelderen, P., de Zwart, J.A., Starewicz, P., Hinks, R.S., Duyn, J.H., 2007. Real-time shimming to compensate for respiration-induced B0 fluctuations. Magn. Reson. Med. 57, 362–368.

Weiskopf, N., Hutton, C., Josephs, O., Turner, R., Deichmann, R., 2007. Optimized EPI for fMRI studies of the orbitofrontal cortex: compensation of susceptibility-induced gradients in the readout direction. Magma 20, 39–49.

Weisskoff, R.M., Kiihne, S., 1992. MRI susceptometry: image-based measurement of absolute susceptibility of MR contrast agents and human blood. Magn. Reson. Med. 24, 375–383.

Yablonskiy, D.A., Haacke, E.M., 1994. Theory of NMR signal behavior in magnetically inhomogeneous tissues: the static dephasing regime. Magn. Reson. Med. 32, 749–763.

Yacoub, E., Shmuel, A., Pfeuffer, J., Van De Moortele, P.F., Adriany, G., Andersen, P., Vaughan, J.T., Merkle, H., Ugurbil, K., Hu, X., 2001. Imaging brain function in humans at 7 Tesla. Magn. Reson. Med. 45, 588–594.

Yacoub, E., Duong, T.Q., Van de Moortele, P.F., Lindquist, M., Adriany, G., Kim, S.G., Ugurbil, K., Hu, X.P., 2003. Spin-echo fMRI in humans using high spatial resolutions and high magnetic fields. Magn. Reson. Med. 49, 655–664.

Yacoub, E., Van De Moortele, P.F., Shmuel, A., Ugurbil, K., 2005. Signal and noise characteristics of Hahn SE and GE BOLD fMRI at 7 T in humans. Neuroimage 24, 738–750.

Yacoub, E., Shmuel, A., Logothetis, N., Ugurbil, K., 2007. Robust detection of ocular dominance columns in humans using Hahn Spin Echo BOLD functional MRI at 7 Tesla. Neuroimage 37, 1161–1177.

Yang, Y., Wen, H., Mattay, V.S., Balaban, R.S., Frank, J.A., Duyn, J.H., 1999. Comparison of 3D BOLD functional MRI with spiral acquisition at 1.5 and 4.0 T. Neuroimage 9, 446–451.

Zhou, J., Golay, X., van Zijl, P.C., Silvennoinen, M.J., Kauppinen, R., Pekar, J., Kraut, M., 2001. Inverse T(2) contrast at 1.5 Tesla between gray matter and white matter in the occipital lobe of normal adult human brain. Magn. Reson. Med. 46, 401–406.

Zou, P., Hutchins, S.B., Dutkiewicz, R.M., Li, C.S., Ogg, R.J., 2005. Effects of EPI readout bandwidth on measured activation map and BOLD response in fMRI experiments. Neuroimage 27, 15–25.